Appl. Phys. B 72, 479–489 (2001) / Digital Object Identifier (DOI) 10.1007/s003400100520

Applied Physics B
Lasers
and Optics

Picosecond laser-induced fluorescence from gas-phase polycyclic aromatic hydrocarbons at elevated temperatures. II. Flame-seeding measurements

F. Ossler*, T. Metz, M. Aldén

Department of Combustion Physics, Lund Institute of Technology, P.O. Box 118, 221 00 Lund, Sweden

Received: 11 July 2000/Revised version: 30 October 2000/Published online: 21 February 2001 –

Abstract. Picosecond laser-induced radiative emission from flames injected with aromatic substances has been measured spectrally and temporally resolved. The measurements were performed in various seeded regions and for different stoichiometric ratios of the surrounding gas. The wavelength of the excitation radiation was 266 nm.

Changes in the lifetime and the spectral composition of the emission were observed with changes in the equivalence ratio and the position in the flame. Considerable agreement with previously reported cell measurements was obtained for those regions close to the injection zone. Temperatures were determined from spectrally and temporally resolved measurements. The comparison with elastic scattering gave reasonable results at low seeding rates for naphthalene, and is hoped to be improved even further in future experiments by increasing the time resolution and the signal-to-noise ratio of the measurements. Downstream and towards the surrounding gas, the lifetimes increased and the spectral profiles shifted and broadened towards the red. This effect increased when the equivalence ratio for the surrounding gas decreased and the oxygen concentration increased.

The study was also directed towards characterizing features in the emission that could be indicative of a transition from the seeded aromatic substance to the formation of soot. An indicator for molecular or particle growth was the composition of the spectral emission in terms of UV, blue and green–yellow bands and the ratio between elastic-scattering signal and total emission signal. Spatially resolved measurements across the seeding region using a gated intensified CCD camera allowed a closer study of the molecular-growth region from the parent aromatic substance seeded to the soot formed. The fluorescence properties of dimers and their cyclodehydrogenated compounds and polymers containing aryl units are also discussed.

PACS: 33; 34; 33.50.-j; 42.62.Fi

*Corresponding author.
(Fax: +46-46/222-4542, E-mail: frederik.ossler@forbrf.lth.se)

Polycyclic aromatic hydrocarbons (PAH) have been the subject of study for many years and several researchers have studied their presence in flames. Reviews and discussions regarding the presence and formation of PAH and soot in different types of combustion can be found in, for example, [1, 2] and references therein. Aromatic substances are considered to be important precursors to soot. Regulations regarding emissions of PAH and particulates from combustion are expected to become more severe in the near future, considering the health aspects associated with these substances. To meet the new regulations the control of the combustion processes to produce less soot and PAH, particularly in urban areas, will be essential. In order to control the combustion process in this respect, one has to probe the early stages of combustion to reduce the rates of aromatic molecular growth and soot formation. The earliest stages in this growth process should then be given by the presence of lighter PAH. Studies have been done on the chemistry involved in the combustion of gas-phase aromatic fuels, mostly by means of chemical probing. Benzene [3–6], phenol [7] and naphthalene [8] are examples of such fuels being used in experiments. Benzene combustion has been studied at different pressure conditions [3–6]. Naphthalene flames have been studied at low pressures using radical scavenging [9]. Bi-aryl reactions have been implicated as important for the formation of PAH and soot in aromatic fuel pyrolysis [10].

Laser diagnostic methods enable in situ on-line probing of different substances during combustion. Fluorescence, elastic scattering/extinction and laser-induced incandescence (LII) are examples of techniques used to monitor aromatic substances, soot volume fractions and size of soot particles [11]. In gas-phase combustion these techniques are easier to use than in the case of bi-phase or multi-phase combustion where scattering from solid- or liquid-phase particles (droplets) may be dominating.

A problem with in situ fluorescence for the identification of different organic substances is the broad and structure-less spectral profiles of polyatomic molecules that make selectivity difficult. Furthermore, a comparison with spectra obtained

at low temperatures may be futile if the properties of the emission change, for example, with temperature. The detection sensitivity also depends on the absorption coefficients and quantum yields, which can be very dependent on the structure of the molecules. In optical probing, the understanding of the fluorescence properties of lighter PAH in flames is therefore of great interest in the study of the early soot formation stages under practical combustion conditions.

In a previous paper [12], which treated the fluorescence properties of some PAH at elevated temperatures (up to 1200 K), it was found that the lifetimes and the spectral profiles of the fluorescence emission depend on the temperature. Consequently, the spectral and dynamic dependence on temperature has to be considered when doing in situ measurements of the fluorescence emission from aromatic substances in flames. In this paper we investigate how two of the substances (naphthalene and pyrene) behave in flame environments characterized by higher temperatures. The substances were injected in the post-flame zone of a premixed atmospheric-pressure CH_4/air flame, which was run at different stoichiometric ratios. The results from the time-resolved and spectrally resolved measurements are reported and discussed. The results are compared with those from the previous paper to determine the possibility to extend the results from the cell measurements to flame conditions. Some information about photophysical properties, stability to flame chemistry and flame temperature was obtained. The investigation also includes spatially and spectrally resolved measurements across different flame regions characterized by different stages in the process of soot formation and a discussion about the identification of the different pyrolysis products.

1 Experiments and results

The set-up used in the experiments is the same as the one used in the previous paper [12], apart from the replacement of the furnace and the cell with a McKenna burner and a seeding part inside the fume box. The fourth-harmonic radiation (266 nm) from the picosecond Nd:YAG laser (Quantel YG572-C), with a pulse duration of 35 ps at the fundamental (1.064 μm), was focused into the probe volume. The fluorescence emission was detected at 90° to the laser radiation. The probe volume was imaged through UV-achromatic lenses, an image-rotating mirror unit, different filters and a beam splitter onto the photocathode of a photomultiplier tube (PMT) (Hamamatsu H5783-4, anode-pulse rise time 0.65 ns) and the entrance slit of a spectrograph/CCD (Jarrel-Ash/Lavision-Flamestar II). In most cases different Schott long-pass filters were used with the PMT. The diode-array detector coupled to the spectrograph used in the previous experiments [12] was replaced with a gated image-intensified CCD camera to allow spatially resolved measurements across the seeded region. The gate of the camera had a minimum gating time of 30 ns and a range of delays with a step of 1 ns. The rise time of the gate was ~ 2 ns. Background-compensated images with different delays and gating times were recorded and stored on a computer during the experiments. Spectral profiles were obtained by summing the CCD counts row-wise, which corresponds to a spatial integration of the fluorescence emission, in the probed volume along the laser beam. The relative spectral sensitivity of the CCD was calibrated using a deuterium lamp and a tungsten lamp. In this way a direct comparison between calibrated spectra obtained from cell measurements and the flame-seeding measurements was possible. The lifetimes were measured using the PMT coupled to an oscilloscope (Tektronix, TDS 620, 2 Gsamples^{-1}, analogue bandwidth 500 MHz). In most cases the lifetimes were obtained by the fitting techniques described in the previous paper using a two-exponential approximation [12]. The short, long and effective lifetimes τ_1, τ_2 and τ_{eff}, respectively, were obtained from the best fits.

The two seeding agents were chosen primarily because they presented the longest lifetime components in the cell measurement. Naphthalene was chosen as the first candidate for seeding due to the low melting and boiling points and relatively low toxicity, which made the seeding less complicated to handle than for the other substances investigated in the previous work.

1.1 The injection zone

Figure 1 shows the region where either naphthalene or pyrene was seeded into the post-flame zone of the premixed methane/ air flame at atmospheric pressure. The seeding region was 8 mm above the surface (bronze plug) of a McKenna burner. The laser radiation could be focused at different heights (h) above the seeder. The experimental set-up was not optimized for collection efficiency of fluorescence emission. Instead particular care was focused on the flexibility in maneuvering the burner position and the detection line

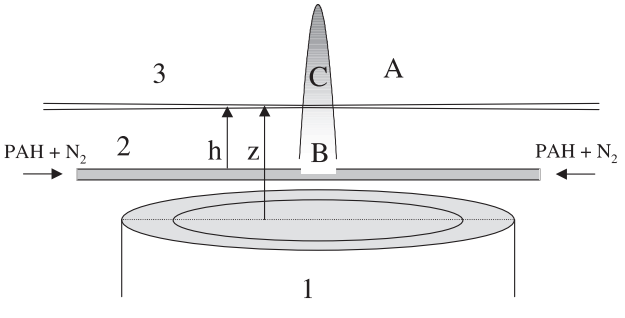

a

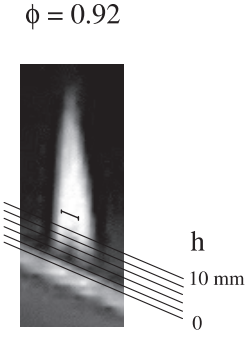

b

Fig. 1. a The injection zone: the aromatic substance (PAH) was carried with nitrogen gas (N_2) into the post-reaction region of a CH_4/air flame (A) above the McKenna-type burner (1). The aromatic gas was conducted inside a Pythagoras (DIN 40865) tube (2) and injected through a slit-shaped orifice 8 mm above the surface of the burner. The zone closest to the injection region (B) was characterized by low luminosity, whereas the zones upstream (C) showed considerable luminosity. By changing the height of the burner the laser radiation (3) was focused in different positions inside the seeded region. **b** Photograph of the injection zone

from outside a fume box, for safety reasons and to diminish the time of data acquisition. For this reason and because of the higher sensitivity, dynamic range and signal-to-noise ratio (S/N), despite the loss in time resolution, the PMT was preferred to the streak camera used in [12].

Table 1 gives the different chemical compositions of the major species, and the corresponding temperature as calculated under the thin-flame approximation [13] for the different conditions under which the burner was operated in the experiments. The height above the burner (z) was 14.8 mm and the total gas velocity changed from ~ 10 to 11 cm s^{-1} when the stoichiometric ratio was changed from 1.01 to 0.92. The substances which show the greatest sensitivity to the stoichiometric ratio are CO, H_2 and O_2. The first two increase while the last one decreases with the equivalence ratio. The upper limit of these concentrations is $\sim 2\%$. The values in the last row are the factors dependent on the refractive index in the expressions for the individual Rayleigh-scattering cross sections, which are used to calculate the cross sections in the post-flame gases relative to air. The results are reported in the last column of the table. Data for the refractive index were obtained from Larsén [14].

In the seeding experiments, gas-phase naphthalene was injected into the premixed flame. Figure 1b shows a photograph of the flame for $\Phi = 0.92$ when seeded with naphthalene at a rate corresponding to 1200 ppm at the injection. The aromatic substance burned above the seeder as a candle-shaped diffusion flame, which was positioned in the post-flame region of the premixed CH_4/air flame. The carrier gas used for the naphthalene seeding was nitrogen. The measurements were performed at different heights in the seeding region and for different equivalence ratios of the premixed flame. Slightly rich flames ($\Phi = 1.01$) produced weak pale orange–red elongated diffusion flames ($\sim$ 7-cm long), whereas lean ones ($\Phi = 0.92$) resulted in luminous yellow flames ($\sim$ 4-cm long). Decreasing the equivalence ratio further shortened the flame (~ 2 cm at $\Phi = 0.89$), and the luminosity decreased and eventually the flame disappeared. In Fig. 1b are marked lines, which indicate different positions (in mm) above the seeder and the extension across the flame probed with the spectrograph/detector.

1.1.1 Concentration and laser power. The seeding rate was controlled by changing the rate of the carrier gas and the temperature of the evaporation chamber. The laser pulse energy was $\sim 60\,\mu$J or 4 GW/cm^2 at high laser power (HP). Measurements were sometimes performed also with low laser power (LP), introducing a 10%-transmission filter in the laser beam before the focus. Comparing the results from the different cases, the sensitivity of the laser-induced emission to laser power was investigated.

In the case of naphthalene seeding the lifetimes and spectral profiles evaluated from measurements corresponding to $\Phi = 1.01 - 1.06$, i.e. at slightly fuel-rich surrounding gas, did not show any significant sensitivity to laser power. On the other hand the lifetimes and spectra were sensitive to the concentration of the seeded substance when using a Schott WG 305 filter (cut-on at 350 nm). In the lower-concentration region the lifetimes were $\tau_1 = 0.30 \pm 0.10$ ns, $\tau_2 = 2.4 \pm 0.2$ ns and $\tau_{\text{eff}} = 0.45 \pm 0.10$ ns. At high seeding rates the lifetimes obtained with WG 305 and GG 435 were two to three times longer and did not differ significantly from each other.

Figure 2 shows some spectral profiles measured for the flame at $z = 14$ mm ($h = 6.3$ mm) for $\Phi = 1.01$ and HP in the region closest to the injection for different naphthalene seeding rates. The intensity of the emission in the visible spec-

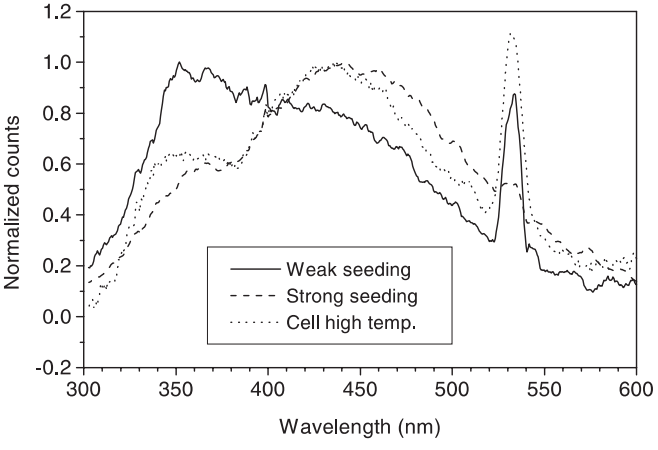

Fig. 2. The spectral profiles, obtained for different seeding rates of naphthalene at $h = 6.3$ mm and for $\Phi = 1.01$, are compared with the spectral profile obtained from the cell measurements at 1205 K and a concentration of $\sim$ 1300 ppm

Table 1. The major species in the post-flame region of a premixed CH_4/air flame. Concentrations, temperature and the real part of the complex refractive index are given. The concentrations of the major species and the temperatures are obtained from Balthasar and Mauss [13]. The refractive indexes are either interpolated or extrapolated to 266 nm from Larsén [14]. The height above the burner was 14.8 mm. The last row gives values proportional to the scattering cross sections for the different species at 298 K and 1 atm. The last column gives the amount of light scattered elastically by the flame gases relative to that expected from air at the same temperature, n is the real part of the complex refractive index

Equivalence ratio	H_2	O_2	H_2O	CO_2	CO	N_2	Temp (K)	Sum concs	Cross section relative to air
0.92 (flame)	3.87×10^{-6}	1.55×10^{-2}	1.76×10^{-1}	8.77×10^{-2}	1.36×10^{-4}	7.20×10^{-1}	1701	1.00	1.10
1.00 (flame)	7.03×10^{-5}	1.70×10^{-3}	1.88×10^{-1}	9.26×10^{-2}	1.98×10^{-3}	7.14×10^{-1}	1713	0.998	1.11
1.01 (flame)	1.03×10^{-4}	8.44×10^{-4}	1.89×10^{-1}	9.22×10^{-2}	3.18×10^{-3}	7.12×10^{-1}	1712	0.996	1.11
1.10 (flame)	1.62×10^{-2}	3.37×10^{-6}	1.87×10^{-1}	8.07×10^{-2}	2.07×10^{-2}	6.95×10^{-1}	1661	1.00	1.09
$(n-1)\times10^6$	152.71	294.53*	278.68*	484.23	371.78	318.93			
$(n^2-1)^2/(n^2+2)^2$ $\times10^8$	1.0364	3.8550	3.4514	10.420	6.1425	4.5196			

* Extrapolated from Larsén [14]

tral region (380–550 nm) increased with the concentration. A spectrum from the high-temperature cell measurements is included for comparison. The peak observed at 532 nm is the contribution from the second-order interference from elastically scattered radiation at 266 nm. The true intensity at the second-order interference should be 1.7 times less than that of the corresponding 532-nm radiation. The relatively strong elastic-scattering signal obtained for the cell is dominated by scattering from the walls of the cell.

The differences in results between flame and cell measurements were stronger for pyrene than for naphthalene. Figure 3 shows the comparison between spectral profiles obtained from flame seeding and cell measurements for pyrene. The flame measurements were done for $h = 6$ mm, $\Phi = 1.02$ and a pulse energy of $\sim 60\,\mu$J, i.e. HP. The gate duration on the CCD was 300 ns compared to 50 ns for the case of the naphthalene measurements. The emission in the UV ($\sim$ 330–390 nm) was stronger for the flame than for the cell measurements. Also, the emission (elastic scattering excluded) in the region 420–600 nm was stronger in the flame and the emission in the region 450–600 nm increased further with the concentration of the seeded pyrene. The concentration of pyrene was estimated to be ~ 1000 ppm.

Figure 4 gives the spectral profiles resulting at different delays on the gate of the CCD for naphthalene, Fig. 4a, and pyrene, Fig. 4b, seeded at a high rate. The measurements were done for $\Phi = 1.03$ and 1.02, respectively, and corresponding gate durations of 50 and 300 ns. High laser power was used and the flame was probed at $h = 6$ mm. In the measurements, a delay of 20 ns on the gate would correspond approximately to the time of arrival of the laser pulse into the probed volume. Ten nanoseconds later the emission in the previously mentioned visible spectral regions becomes dominating. Consequently the lobe of the profile on the long-wavelength side observed at short delays for naphthalene seeding presents a more long-lived emission than at the shorter wavelengths, in accordance with the results from previously reported cell measurements [12]. Typical lifetimes measured with a Schott WG 305 filter were $\tau_1 = 0.55 \pm 0.10$ ns, $\tau_2 = 3.3 \pm 0.3$ ns and $\tau_{\text{eff}} = 0.8 \pm 0.1$ ns for pyrene. In the visible, using a GG 435 filter, the lifetimes were $\tau_1 = 0.90 \pm 0.10$ ns, $\tau_2 = 4.3 \pm 0.1$ ns and $\tau_{\text{eff}} = 1.45 \pm 0.10$ ns. This value for τ_2 was slightly shorter than found for the corresponding naphthalene seeding reported above (5.4 ns). In the case of pyrene, measurements were also made using a Schott OG 590 filter, which resulted in increased lifetimes of $\tau_1 = 1.10 \pm 0.10$ ns, $\tau_2 = 7.7 \pm 0.6$ ns and $\tau_{\text{eff}} = 1.50 \pm 0.10$ ns. These long lifetimes belonged to an emission which was hardly captured with the spectrograph and could have been due to PAH formed at high seeding rates with pyrene.

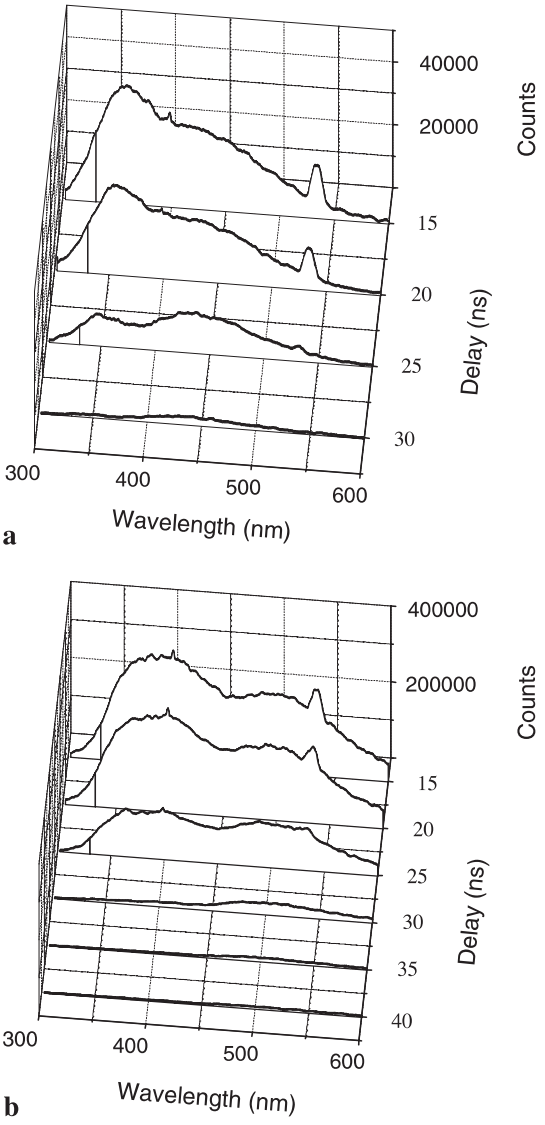

Fig. 4a,b. Spectral emission from naphthalene (**a**) and pyrene (**b**) at different delays on the gate: the conditions were **a** $\Phi = 1.03$, high laser power, $h = 6.3$ mm, gate duration 50 ns, and **b** $\Phi = 1.02$, high laser power, $h = 6.0$ mm, gate duration 300 ns

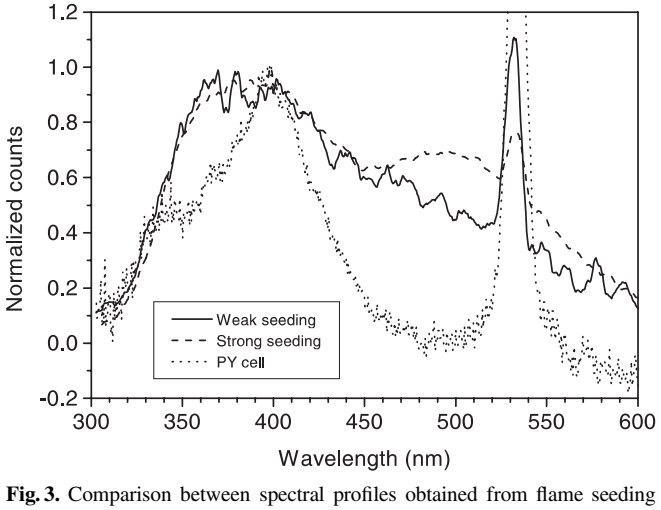

Fig. 3. Comparison between spectral profiles obtained from flame seeding and cell measurements of pyrene. For the flame measurements the conditions were $\Phi = 1.02$, high laser power and $h = 6.0$ mm

1.1.2 Temperature. In the previous cell measurements for temperatures up to 1200 K [12], the spectral and temporal properties of the fluorescence were found to be sensitive to temperature. The results from the cell measurements were used as a starting point for the flame-seeding experiments, i.e. to study the fluorescence properties at even higher temperatures. Naphthalene and pyrene were chosen and the comparison was limited to the seeding region closest to the

injection under oxygen-free conditions. In this probed region, the composition was dominated by nitrogen buffer and the parent aromatic substance. Higher up in the seeding region, pyrolysis and the diffusion between the seeded gas and the surrounding gas increased. The comparison was assumed to be less appropriate in particular for $\Phi < 1$, when the oxygen concentration in the surrounding gas was considerable (see Table 1).

The spectral and temporal properties of naphthalene fluorescence in the cell measurements showed a monotonic dependence on temperature, indicating that temperatures can, in principle, be determined from fluorescence measurements. Apart from the effects of dual fluorescence, the same thing can be said for pyrene. Temperatures evaluated from different fluorescence measurements can be compared among themselves and with other independent temperature measurements to determine how well the properties of the fluorescence emission at flame temperatures agrees with the predictions based on the high-temperature cell measurements. The results are reported in Table 2. The fluorescence-based measurements relied on extrapolation of the behavior against temperature that was observed for the cell measurements in the high-temperature region, up to temperatures around 1200 K. The errors given in the evaluated temperatures correspond to the estimated precision considering the precision ($\pm 1\sigma$) of the data obtained in the calibration measurements [12] used for the extrapolation and the precision of the data for the flame.

An independent measurement of the temperature of the non-seeded flame 15 mm above the plug of the burner ($h =$ 7 mm) was done. The temperature was determined from measurements based on Rayleigh-scattered light (see, for example, [11]). The scattered light was measured with the PMT in combination with an interference filter (265 nm, 10-nm bandwidth). The temperature evaluated was 1590 ± 30 K for $\Phi = 1.0$, taking into account effects from differences in Rayleigh cross sections and laser extinction between flame gases and air.

The temperature in the seeded flame was determined from the spectral properties of the fluorescence in the early seeding region. However, the evaluation was based on three different points of the spectral profiles: the leading (LE50) and falling edges (FE50) (50% of maximum) as well as the maximum positions. The evaluations were based on equations of temperature against spectral positions that were obtained from the inversion of a second-order polynomial fit to the data from the cell measurements. From the corresponding spectral positions evaluated from the flame-seeding measurements (first 10 ns of the fluorescence emission), temperatures were determined by taking into account differences in the spectral sensitivity of the two different detectors used in the different experiments. The results from the maximum and the falling edge of naphthalene are affected by the emission from the pyrolysis products and are therefore deteriorated, but have been reported in Table 2 to give an indication of the deviation from the evaluation based on the leading edge. The results for pyrene have not been reported since none of the evaluations gave reasonable results.

The temperatures were also obtained from the lifetimes using the negative-exponential dependence of lifetimes on temperature obtained from the cell measurements. The temperatures in Table 2 are the highest temperatures obtained from the measurements. Evaluations were also based on the effective lifetimes which, however, were not supposed to be strictly negative-exponential in the dependence with temperature. Since long-pass filters were used in these measurements, and the lifetimes generally increased with concentration and emission wavelength, the temperatures obtained were expected to be lower than the true temperatures. From the previous paper [12] the precision and accuracy due to the evaluation of the short lifetimes (200–400 ps) were estimated to be ±30%. Further sensitivity analysis showed that at a S/N of 50 the increase in τ_1 was 10%–20%, which corresponds to a systematic error in the evaluation of the temperature of 20–40 K downwards. In any case, for naphthalene, the agreement between the results from LE50 and the lifetime-based results was within the precision of the evaluation. However, the long lifetimes in the naphthalene-seeding experiments, due to contributions from the longer-lived emission from pyrolysis products, yielded lower temperatures (~ 100 K) than the corresponding short ones. The correspondence between short and long lifetimes for pyrene was better; in fact no significant differences were found in the temperatures evaluated. On the other hand, large differences in temperatures were obtained both between the spectrally based evaluations themselves and the spectrally based ones compared with the temporally based results. In any case it should be noted

Table 2. Temperatures evaluated from the spectrally and temporally resolved measurements, measured scattering and calculations on the flame gases. The first and next three rows show the results from spectrally and temporally resolved measurements respectively. A Schott WG 305 filter was used for the temporally resolved measurements, the results of which are shown for the highest temperatures obtained. The last two rows show the results from elastic-scattering measurements and kinetic calculations. The temperature dependences used were obtained from the cell measurements [12] using different filters in front of the PMT

Evaluation	Temperature (K) Naphthalene	Pyrene	Non-seeded
LE50	1400 ± 100	*	–
Max	1300 ± 110	*	–
FE50	1700 ± 220	*	–
τ_1	1450 ± 70[a] 1380 ± 70[b]	1370 ± 60[c]	–
τ_2	1330 ± 70[a] 1300 ± 60[b]	1380 ± 50[c]	–
τ_{eff}	1390 ± 50[a] 1350 ± 40[b]	1350 ± 40[c]	–
Elastic scattering	–	–	1590 ± 30[d]
Calculations	–	–	1680 ± 30[e]

[a] CVI 350,
[b] CVI 325,
[c] Schott WG 305.
[d] The elastic-scattering measurements were done for non-seeded flame gases at $z = 15$ mm for $\Phi = 1.0$.
[e] The kinetic calculations [13] did not consider cooling from seeder and the injected gases.
* Errors were considered too large to give significant results.

that the results on pyrene obtained from the cell measurements rely on less data and data with lower S/N than for the case of naphthalene. The changes of the spectrum for pyrene did not follow the same behavior as that of naphthalene. For instance the appearance of the so-called dual fluorescence [15, 16] in the UV-spectral region with temperature also makes the second-order polynomial fit probably less suitable.

The accuracy of the fluorescence-based method was not compared to vibrational coherent anti-Stokes Raman scattering (CARS), which is known to have an accuracy of a few percent, or thermocouple measurements. The implementation of CARS would have required additional laser equipment and could have affected the compatibility of the two different measurements for the configuration of the set-up used. Thermocouple measurements were not performed, since the injection zone was very narrow and the metallic surface could have interfered with the pyrolysis present close to the injection.

1.2 Different seeding regions

Different parts of the aromatic diffusion flame were studied keeping the laser beam at a certain height above the burner and changing the stoichiometric ratio of the surrounding gas and consequently shrinking or stretching the aromatic flame. Another way was to change the vertical position of the laser focus across the flame and thereby study the evolution downstream. The influence of laser power on the emission was also investigated in the different regions.

1.2.1 Different stoichiometric ratios. More developed regions of the pyrolysis and soot formation entered the probe volume as the equivalence ratio was decreased, due to the shrinking of the aromatic flame. The lifetimes measured with the PMT and a WG 305 filter at HP increased when equivalence ratio decreased.

Figure 5a gives spectral profiles obtained for $h = 5.1$ mm for naphthalene seeding at different stoichiometric ratios of the premixed gas. In the spectral profiles, the counts at the positions of the ends of the wings of the elastic scattering were used to linearly interpolate the inelastic emission in the scattering region. After this procedure the difference between total counts and interpolated counts was defined as the elastic scattering and was removed from the spectrum. Based on the spectral structures for the monomer and the pyrolysis products, the inelastic emission was integrated over three wavelength regions, 300–400 (UV), 400–500 (blue–green) and 500–600 nm (green–yellow). For simplicity we will name them by the respective colors at the upper limit, violet (V), green (G) and yellow (Y). The relative contribution of inelastic emission to the different regions as well as the contribution from elastic scattering to the total emission was calculated. The normalized spectral numbers (NSN_{TE}) of the total emission (TE) obtained in this way are given in Fig. 5b. The corresponding normalized spectral numbers NSN_{IE} of the inelastic emission (IE), i.e. excluding elastic scattering, are given in Fig. 5c. Different types of spectra (I–IV) can be defined based on different combinations of these numbers, the limits of which are given by the vertical lines in the same figure. Types I and II refer to spectra dominated by V and

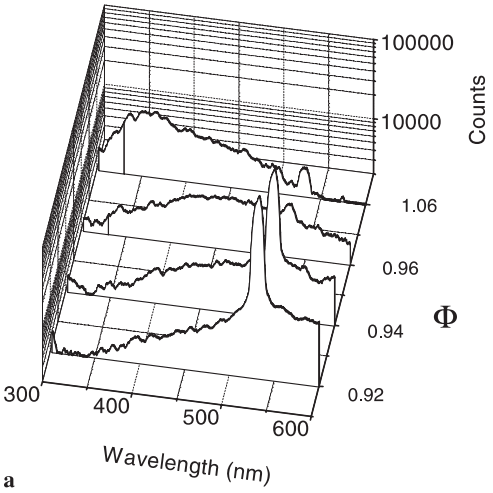

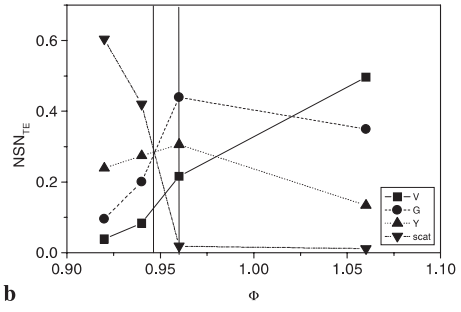

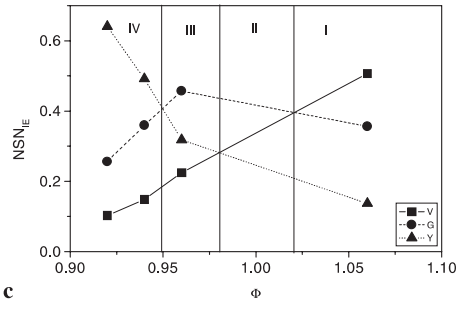

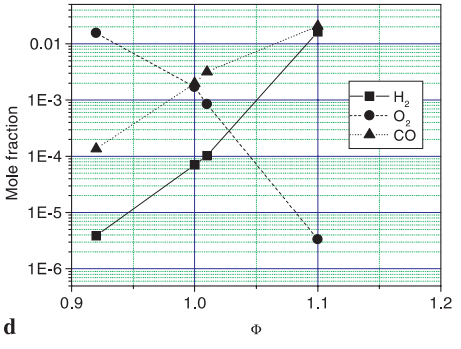

Fig. 5. a Spectral emission for different equivalence ratios at $h = 5.1$ mm and for naphthalene seeding and high laser power presented on a logarithmic intensity scale. The NSN_{TE} representing intensity of the emission in the different spectral regions are given in **b** when elastic scattering is included in the emission. The *dotted vertical lines* mark out the region where a rapid increase is observed in the intensity of the elastic scattering. In **c** are given the corresponding NSN_{IE}, where the contribution from elastically scattered light has been excluded. The regions I–IV indicate the different types of spectra that appear in the measurements and that are later used to characterize the aromatic flame. The concentrations of these substances in the surrounding gas, which were most sensitive to changes in the equivalence ratio [13], are given in **d**

G in that order and G and V respectively. Type III corresponds to spectra dominated by G and Y in that order, and it appears slightly before the intensity of the elastic scattering starts to increase considerably. The NSN_{IE} for (V, G, Y) is here in a narrow region (±0.02) around (0.21, 0.42, 0.36) when a rapid increase in the scattering is observed. Finally for type IV the emission is dominated by Y and G in that order. Usually the scattering is strong or dominating in such regions. Figure 5d gives the concentrations of the species in the surrounding gas (from Table 1) that are most sensitive to Φ.

1.2.2 Laser power. For soot-containing yellow and luminous flames, for example for $\Phi = 0.93$ and $\Phi = 0.92$, the lifetimes at HP were considerably longer than for LP. Figure 6a and 6b show spectra obtained for the sooty region for different delays on the gate for the HP and LP conditions when $\Phi = 0.92$ for naphthalene seeding. A Schott WG 305 was used to suppress the signal from elastic scattering. There are considerable differences in the temporal evolution of the emission between the low-power and high-power cases. In the LP case, Fig. 6b, the spectral composition changes very rapidly at the beginning, in contrast to the HP case, Fig. 6a. Investigating the emission in different time windows, one observes a transition of spectra from type III to type IV in the LP regime with increasing delay (going from the first ∼ 5 to the next 10 ns of the emission). In the HP regime the spectra are always of type IV. Low laser power yields shorter lifetimes than for high laser power, as is shown in Fig. 7a for the case when a WG 305 was used in front of the PMT. One should, however, notice that the spectral measurements revealed a long-lived emission at wavelengths longer than 450 nm for the LP case also and that it was on the time scale of microseconds or longer. The lifetimes for LP measured with the PMT were in the range $\tau_1 = 0.4$–1.6 ns, $\tau_2 = 5.5$–8 ns and $\tau_{eff} = 0.9$–2.3 ns. At HP the profiles were in many cases better-described by a three-exponential fit. The lifetimes were then $\tau_1 = 1.7 \pm 0.3$ ns, $\tau_2 = 16 \pm 3$ ns, $\tau_3 = 120 \pm 2$ ns and $\tau_{eff} = 34 \pm 1$ ns. In Fig. 7b the short lifetime at HP increases considerably with the emission wavelength. The lifetimes reported were obtained from the decay with a two-exponential fit without using the convolution/deconvolution scheme described in the previous paper [12]. The short-lifetime components obtained in this way are longer, but have been chosen to facilitate the comparison with the results from measurements at longer wavelengths where evaluations on the decay gave higher stability in the evaluations, in particular when an RG 715 (cut-on at 715 nm) filter was used. Three-exponential fits resulted in lifetimes between 3 and 6 ns. If one calculates an effective

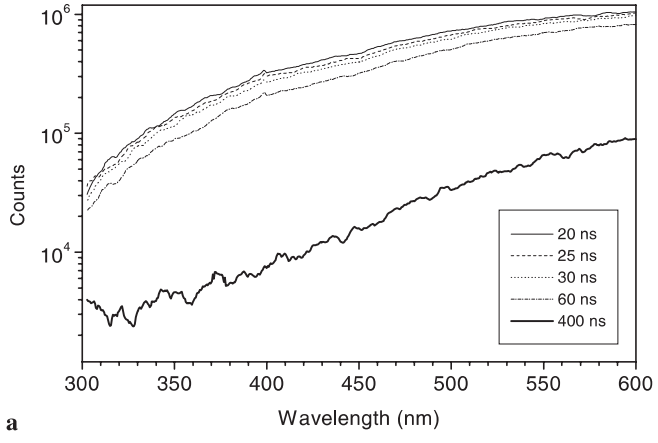

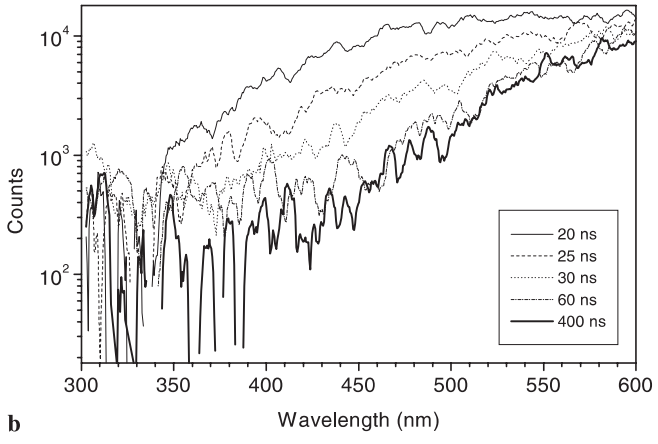

Fig. 6a,b. Spectral emission for $\Phi = 0.92$ at 7.2 mm above the injector measured for naphthalene seeding using a Schott WG 305 long-pass filter in front of the entrance slit of the spectrograph and for different delays: **a** pulse energy, ∼ 60 μJ, and **b** ∼ 6 μJ

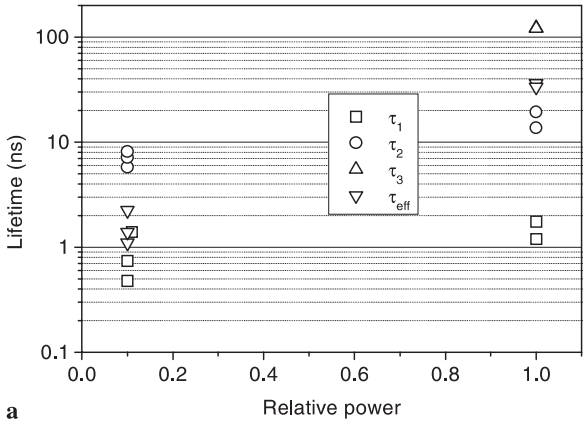

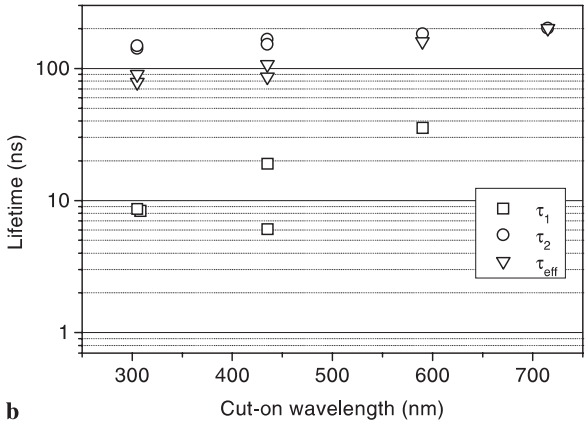

Fig. 7a,b. Lifetimes measured for $\Phi = 0.92$ at 7.2 mm above the injector for naphthalene seeding: **a** a Schott WG 305 long-pass filter was used in front of the PMT and different pulse energies were used, ∼ 60 μJ and ∼ 6 μJ. **b** Lifetimes measured with different long-pass filters at 60 μJ

lifetime from the two fastest decays obtained from the three-exponential fit one obtains a value close to 8 ns; thus not far from the short lifetime obtained with the two-exponential fit of the decay. Changing the Schott filters from WG 305 to OG 590, τ_1 increased from a couple of nanoseconds to above 30 ns. No short lifetime was revealed using an even higher cut-on wavelength-filter (Schott RG 715). Although the different choices of the resolution of the oscilloscope affected the early part of the decay differently, the observed differences in the lifetimes were too large to be explained from such an influence. The long lifetime was also observed to increase. It increased from 120 ns using WG 305 to 200 ns with RG 715. The fast-decaying emission observed at LP could be due to fluorescence, since it is supposed to be much faster than LII. Although LII is not supposed to present a strict one-exponential decay [17], lifetimes of the order of 100 ns normally have been measured with ns-laser-based systems [18]. The lifetime is known to increase with the size of the primary particle. At the laser fluences used ($\leq 80\ \mathrm{mJ/cm^2}$) LII should increase rapidly with laser power, see, for example, [19] and references therein. That may explain why no fluorescence was observed at high laser power because it became much weaker with respect to LII.

1.2.3 Different heights. In order to study the possible transition stages between parent naphthalene and soot, the laser-induced emission was detected spectrally and spatially resolved along the laser beam across the seeding region for the flame pictured in Fig. 1b. The evolution of the aromatic substance seeded, towards the formation to soot, can be seen by comparing the results for the spatial distribution of the measured spectral properties reported in Fig. 8. The different zones characterized according to the properties of the emission as defined above in Sect. 1.2.1 can be considered to represent different stages in the process towards the formation of soot.

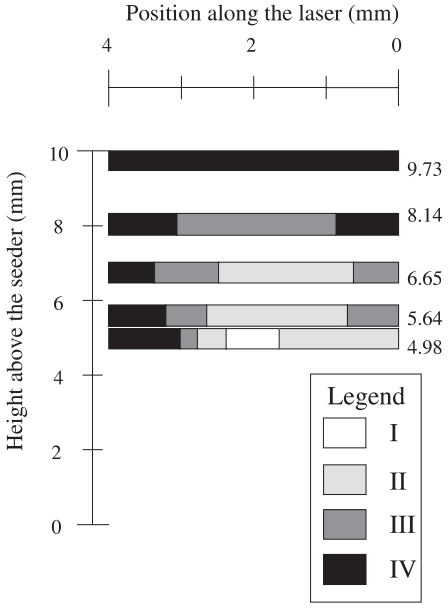

Fig. 8. The spectral map of an aromatic flame obtained for naphthalene seeding for high laser power. The same flame is seen in Fig. 1b. The spectral identification of the different flame zones (I–IV) is based on the definition given in Fig. 5c. Zones I, II, III and IV are characterized by different stages in the pyrolysis and soot formation

2 Discussion

2.1 Temperature

As has been demonstrated by Ni and Melton [20] the fluorescence lifetimes of naphthalene can be used to measure the temperature (up to 720 K) in seeded nitrogen gas flows. The results presented in the previous paper [12] show that other aromatic substances or PAH may also be used for temperature determination up to ~ 1200 K. Results presented in this paper indicate that it could be measured in seeded flames in regions absent of oxygen and with a low degree of pyrolysis. However, the major decay components have lifetimes considerably below 1 ns; therefore streak cameras with sufficient S/N in the detection should be used. The errors given in the evaluated temperatures correspond to the estimated precision considering the precision ($\pm 1\sigma$) of the data obtained in the calibration measurements [12] used for the extrapolation and of the precision of the data measured for the flame.

The temperatures evaluated from the short lifetimes agree well between naphthalene and pyrene. The agreement between evaluations based on lifetimes and the leading edge of the spectrum was within the precision of the evaluation, apart from the case of pyrene due to the appearance of dual fluorescence. The contribution from the longer-lived red-shifted fluorescence from pyrolysis products partially explains why the flame temperatures evaluated from the lifetimes measured with the broadband filters are expected to be lower than the true temperatures. Due to the same contributions, the evaluation based on FE50 resulted in higher temperatures. For pyrene seeding the lifetimes of this emission were slightly shorter than for naphthalene seeding and they were closer to the values obtained for the corresponding monomer (considering the results from the cell measurements [12]). This property may explain the better agreement between temperatures that were evaluated from the short and long lifetimes.

Similarities in the evaluated temperatures suggest that the high-temperature trend of the fluorescence, observed for naphthalene and pyrene in the cell measurements, is maintained in the flame investigated. The discrepancy in temperatures between fluorescence measurements, elastic scattering and calculations can be explained. The scattering measurements were done without any seeding and therefore a higher temperature was measured. The calculations, which did not include the heat sink caused by the burner surface, resulted in higher temperatures.

The precision and the accuracy in the evaluated temperatures are supposed to improve with increasing precision and accuracy in the calibration. The lifetimes used for the evaluation should be measured with properly chosen band-pass filters to minimize the interference from pyrolysis products, which are formed downstream in the early seeding region.

2.2 Fluorescence properties and pyrolysis products

Pyrolysis of naphthalene and pyrene is known to produce substances such as binaphthyls, perylene, benzofluoranthenes, ternaphthyl and terylene [21, 22], and bipyrenyl and dibenzopyrenes [21, 23]. In accordance with results from naphthalene measurements at high temperature [24], binaphthyls dominated in the depositions of the cell outlet.

Unfortunately, very little is known about the fluorescence properties of the pyrolysis products in the gas phase and at high temperature. Measurements on pure substances have, to our knowledge, not been reported under these conditions. There are results for liquid solutions at room temperature or the low-temperature solid phase for some of the species, see, for example, [21, 22, 25–27].

The efficiency with which different substances can be detected is important for the analysis of the fluorescence. The efficiencies during the entire duration of emission and in the earliest part of the decay can be defined as $\varepsilon \times \eta$ and ε/τ_0 respectively. ε, η and τ_0 are the molar extinction coefficient, the fluorescence quantum yield and the natural lifetime [25]. Using reference data from liquid room-temperature solutions, one should consider spectral red shifts and shortening of fluorescence lifetimes following an increase of temperature in the gas phase [12] and also changes due to transition from liquid to gaseous solution. However, perylene fluorescence has been found to be rather temperature-insensitive [28].

Mono-ring aromatic species should have their peak fluorescence at lower wavelengths than naphthalene. In our measurements no clear evidence of an increase in the UV emission with the seeding rate was found.

In the early pyrolysis region (I and II), dimers should fluoresce to the red of the monomers. However, a comparison between reference data from liquid solution, the results from the cell and flame-seeding measurements and reports on perylene [28] from the gas phase (between 495 and 633 K) indicate that the red-shifted emission assigned to early stage pyrolysis agrees best with cyclodehydrogenated forms. Strong red shifts with increasing temperature are needed to attribute the red-shifted emission seen in the early pyrolysis region to the dimers. In previous studies [12, 28] strong red shifts led to a strong decrease in the fluorescence quantum yield and despite the higher concentrations with respect to the cyclodehydrogenated forms [9, 10, 22, 24] during pyrolysis, emission from dimers should be weak. Furthermore, the stability of energy levels should decrease more rapidly with temperature for dimeric than complete aromatic structures. The efficiency for perylene detection relative to naphthalene should be 200 or 300 times larger depending on whether the comparison is based on the long or effective lifetime of naphthalene. With high collection efficiency in the set-up one should reasonably reach detection levels of sub-ppm for perylene in flames.

Fluorescence quantum yields of the other cyclodehydrogenated substances related to binaphthyl (benzofluoranthene) and bipyrenyl (dibenzo-peropyrene) have not been reported yet. Regarding the spectral properties of the emission, the agreement with the red-shifted emission is good, assuming a sensitivity to temperature similar to that of perylene.

Fluorescence from ionized species produced by two-photon ionization should not be easily revealed [12]. C_2 fluorescence from UV laser-induced fragmentation [29] was not evidenced. Excimers should hardly be present. At flame temperatures the vibrational energy contained in the bonds responsible for the excimer formation is much larger than the binding energies given in [30, 31]. In addition, the time between two consecutive collisions between monomers should be orders of magnitude longer than the electronic lifetimes measured in the experiments. Steric conditions should also have inhibiting effects.

2.3 The characterization of different-size groups

For naphthalene seeding, naphthalene monomers dominate in the injection zone and the dimers and the corresponding cyclodehydrogenated products are progressively formed downstream in regions I and II. These regions are characterized by molecules containing two to five aromatic rings. In principle one can regard the position downstream from the injection in the early seeding region as a time coordinate with a time scale of the order of 10 ms/mm. This means that much of the early pyrolysis products (4–5 aromatic ring units) are formed in the time period between 10 and 60 ms after the injection of naphthalene into the flame.

In region III the emission characteristic of naphthalene has disappeared and the emission shows a considerable contribution from emission in the region between 500 and 600 nm. Terylene, an eight-ring aromatic molecule, is a molecule that can contribute to the emission. In this region there are zones where particle inception has not yet started, e.g. see the curve for $\Phi = 0.96$ in Fig. 5a, where the emission is primarily from molecules and the contribution from elastic scattering has only increased slightly.

In zone IV the contribution from elastic scattering is strong and soot particles are being formed or start to agglomerate. At low laser power, the emission during the first 5 ns was between 370 and 600 nm, and after the next 5 ns above 400 nm, consistent with emission from five-ring structures. However, according to Sarofim et al. [10] only a relatively small number of four- to six-ring compounds persist at high temperatures.

The presence of soot is easily identified by the appearance of strong elastic scattering of the laser radiation and the presence of LII at fluences above some given threshold. The threshold for LII interference in PAH fluorescence measurements in sooty environment has been considered to be $\sim 5\,\mathrm{MW/cm^2}$ for a 10-ns pulsed laser operating in the visible or UV [32]. This corresponds to a fluence of $50\,\mathrm{mJ/cm^2}$. In our measurements strong LII was characterized by long lifetimes that increased to values between 100 and 200 ns and it was observed without any trace of fluorescence at a fluence of $\sim 80\,\mathrm{mJ/cm^2}$. At $\sim 8\,\mathrm{mJ/cm^2}$ fluorescence was assumed to be the relatively fast decaying emission ($\tau \approx 7$–8 ns) measured with the PMT. The spectrally resolved measurements showed in both cases an additional long-lived emission that was strongly red-shifted. Lifetimes of the order of tens of microseconds or longer were probably too long to be detected in the time window used with the PMT. The nature of this emission is not yet understood, but one possibility could be phosphorescence from PAH.

2.4 Future studies

The fluorescence properties of many substances remain to be investigated, e.g. benzoic structures, phenanthrene, acenaphthene, dimers, polymers, larger PAH such as perylene and other cyclodehydrogenated compounds, which are expected to have high fluorescence quantum yields and relatively short lifetimes at flame temperatures. The temperature dependence of the spectrally resolved absorption of the different substances is also of importance and should be investigated.

Structures containing both aromatic and aliphatic units have been suggested to appear in some combustion situations [33, 34]. Polymeric structures or chainlike structures, which present high fluorescence quantum yields and short fluorescence lifetimes in room-temperature liquid solutions, would be interesting to investigate at high temperatures to see if these properties are maintained. These substances could be among the ones most easily detected in combustion situations, although one has to consider the possibility of strong internal quenching for polymeric structures at high temperature.

Alternative methods to improve the signal yield for measurements in flames should be investigated. Delayed fluorescence was obtained by Borisevich [35] in low-pressure vapor by inverse singlet–triplet transfer induced by CO_2 laser radiation after UV excitation. Although this technique is supposed to work at a few Torr of pressure and the signal decreases with an increase in pressure it should still be interesting to investigate the possibilities to apply it in combustion situations at higher temperatures and higher pressures. Pump–probe techniques using short laser pulses in the picosecond or femtosecond regime are some methods also worth investigating.

3 Conclusions

In the measurements described naphthalene or pyrene was seeded about 5 to 7 mm above the reaction zone of a premixed methane/air flame at atmospheric pressure. The aromatic flame burning in the post-flame region of the premixed flame was controlled by changing the stoichiometric ratio of the premixed gas. The soot-formation process in the aromatic flame was sensitive to the composition of the post-flame gas where the presence of CO, H_2 and O_2 changed between roughly 0 and 2%. The greatest effect was presumably caused by O_2. The aromatic flame shortened and became more luminous as the stoichiometric ratio decreased until the flame vanished. The temperatures under the different conditions were estimated to vary between 1300 and 1700 K throughout different regions in the aromatic flame.

Fluorescence from naphthalene-seeded flames in the early seeding region follows the behavior with temperatures described by the high-temperature cell measurements well. The agreement between temperature indications based on the leading edge of the spectral profiles and lifetimes of the fluorescence was within the precision of the evaluation. So also was the agreement for lifetime-based evaluations between naphthalene and pyrene seeding. However, contributions from pyrolysis products should be reduced as much as possible using narrow band-pass filters. The accuracy of the method should be tested with, for example, vibrational coherent anti-Stokes Raman scattering on N_2. Temperatures with an accuracy of a few per cent should be obtained when nitrogen is used as a carrier gas for the seeding.

A streak camera with sufficiently high signal-to-noise ratio in the detection has to be used to resolve the fast dynamics, which would allow a more accurate study and identification in the early seeding region when using naphthalene and pyrene. There is also the interest to use other PAH as seeding agents in order to study the process of soot formation.

Results show the possibility to identify different regions of the aromatic flame by spectral mapping and thereby catch different stages in the soot formation from the parent substance to soot. It should be possible to select different size groups through a combination of temporal and spectral selection of the emission with excitation at 266 nm. An improved selectivity should be obtained by changing the wavelength of the excitation as well. The results from 266-nm excitation on naphthalene-seeded flames indicate sub-nanosecond temporal selection in the UV spectral region for aromatic substances with up to 3–4 condensed rings and species twice that large in the time scale around 1 ns and in the visible spectral region below 600 nm. It is more difficult at this stage to determine in what region larger aromatic molecular structures in the flame should be selected in terms of wavelengths and time intervals. There is also the remaining question of how important phosphorescence is for the detection.

The laser fluences used when LII was dominating and for the case when short-lived emission from possible PAH was observed were $\sim 80\,\mathrm{mJ/cm^2}$ and $8\,\mathrm{mJ/cm^2}$, respectively. Typical values of the long-lifetime components measured with the photomultiplier tube were 100–200 ns and 5–8 ns in respective cases. Spectrally resolved measurements also showed a strongly red-shifted very long-lived emission with lifetimes superior to microseconds of undetermined nature, maybe phosphorescence.

Acknowledgements. We want to give a special thank you to Michael Balthasar and Fabian Mauss for kindly having performed the kinetic calculations. This work was supported financially by the Swedish Research Council for Engineering Sciences (TFR) and the Swedish Board for Industrial and Technical Developments (STEM).

References

1. B.S. Haynes: In *Fossil Fuel Combustion*, ed. by W. Bartok, A.F. Sarofim (John Wiley, New York 1991) p. 261
2. *Soot Formation in Combustion*, ed. by H. Bockhorn (Springer, Berlin 1994)
3. W.J. Grieco, A.L. Lafleur, K.C. Swallow, H. Richter, K. Taghidzadeh, J.B. Howard: In 27th Int. Symp. on Combustion (The Combustion Institute, Boulder (Co) 1998) p. 1669
4. M. Hamida, A. Fonseca, R. Doome, E. De Hoffman, P.A. Thiry, J.B. Nagy: In 27th Int. Symp. on Combustion (The Combustion Institute, Boulder (Co) 1998) p. 1663
5. A. Tregrossi, A. Ciajolo, R. Barbella: Combust. Flame **117**, 553 (1999)
6. H. Böhm, H. Jander, D. Tanke: In 27th Int. Symp. on Combustion (The Combustion Institute, Boulder (Co) 1998) p. 1605
7. C. Horn, K. Roy, P. Frank, T. Just: In 27th Int. Symp. on Combustion (The Combustion Institute, Boulder (Co) 1998) p. 321
8. S.D. Klotz, K. Brezinsky, I. Glassman: In 27th Int. Symp. on Combustion (The Combustion Institute, Boulder (Co) 1998) p. 337
9. J. Griesheimer, K.-H. Homann: In 27th Int. Symp. on Combustion (The Combustion Institute, Boulder (Co) 1998) p. 1753
10. A.F. Sarofim, J.P. Longwell, M.J. Wornat, J. Mukherje: The role of biaryl reactions in PAH and soot formation, In *Soot Formation in Combustion*, ed. by H. Bockhorn (Springer, Berlin 1994) p. 485
11. A.C. Eckbreth: *Laser Diagnostics for Combustion Temperature and Species*, 2nd edn. (Gordon & Breach, Amsterdam 1996)
12. F. Ossler, T. Metz, M. Aldén: Picosecond laser-induced fluorescence from gas-phase aromatic hydrocarbons at elevated temperatures. I. Cell measurements, Appl. Phys. B **72**, 465 (2001), DOI 10.1007/s003400100519
13. M. Balthasar, F. Mauss: private communication
14. T. Larsén: In *Landolt-Börnstein*, 6th edn., Vol. II: Eigenschaften der Materie in ihre Aggregatzustanden (Springer, Berlin 1962) Chapt. 8 (Optische konstanten), pp. 6–889
15. J.B. Birks: In *Organic Molecular Photophysics* Vol. 1, ed. by J.B. Birks (John Wiley, London 1973), Chapt. 1; M. Stockburger: In *Organic Molecular Photophysics*, ed. by J.B. Birks (John Wiley,

London 1973) Vol. 1, Chapt. 2; J.B. Birks: *Photophysics of Aromatic Molecules* (John Wiley, London 1970)
16. D.S. Coe, J.I. Steinfeld: Chem. Phys. Lett. **76**, 485 (1980); D.L. Peterson, F.E. Lytle, N.M. Laurendeau: Opt. Lett. **11**, 345 (1986); D.L. Peterson, F.E. Lytle, N.M. Laurendeau: Appl. Opt. **27**, 2668 (1988)
17. S. Will, S. Schraml, K. Bader, A. Leipertz: Appl. Opt. **37**, 5647 (1998)
18. T. Ni, J.A. Pinson, S. Gupta, R.J. Santoro: Appl. Opt. **34**, 7083 (1995); B. Mewes, J.M. Seitzman: Appl. Opt. **36**, 709 (1997)
19. R.L. Vander Wal, K.A. Jensen: Appl. Opt. **37**, 1607 (1998)
20. T. Ni, L.A. Melton: Appl. Spectrosc. **50**, 1112 (1996)
21. E. Clar: *Polycyclic Hydrocarbons* Vol. 2, (Academic, London 1964)
22. K.F. Lang, H. Buffleb, J. Kalowy: Chem. Ber. **90**, 2888 (1957)
23. K.F. Lang, H. Buffleb: Chem. Ber. **90**, 2894 (1957)
24. A. Ciajolo: private communication
25. I.B. Berlman: *Handbook of Fluorescence Spectra of Aromatic Molecules*, 2nd edn. (Academic, New York 1971)
26. H. Dreeskamp, E. Koch, M. Zander: Z. Naturforsch. A **30**, 1311 (1975)
27. J.M.G. Martinho, J.P. Farinha, M.N. Berberan-Santos: J. Chem. Phys. **96**, 8143 (1992)
28. V.V. Gruzinskii, S.V. Davidov, A.V. Kukhto: J. Appl. Spectrosc. **46**, 573 (1987); V.V. Gruzinskii, K.M. Degtyarenko, T.N. Kopylova, V.T. Pavlova: Izv. Vyssh. Uchebn. Zaved. Fiz. **4**, 118 (1984)
29. P.-E. Bengtsson: On the use of laser techniques in the diagnostics of sooting flames, Dissertation Thesis, Lund (1991)
30. B.K. Selinger: Aust. J. Chem. **19**, 825 (1966)
31. J.B. Birks, D.J. Dyson, I.H. Munro: Proc. R. Soc. London, Ser. A **275**, 575 (1963); J.B. Birks, M.D. Lumb, I.H. Munro: Proc. R. Soc. London, Ser. A **280**, 289 (1964)
32. P.-E. Bengtsson, M. Aldén: Appl. Phys. B **60**, 51 (1995)
33. A. D'Anna, A. D'Alessio, P. Minutolo: Spectroscopic and chemical characterization of soot inception processes in premixed laminar flames at atmospheric pressure, In *Soot Formation in Combustion*, ed. by H. Bockhorn (Springer, Berlin 1994) p. 485
34. A. D'Anna, A. Violi: In 27th Int. Symp. on Combustion (The Combustion Institute, Boulder (Co) 1998) p. 425
35. N.A. Borisevich: Acta Phys. Pol. A **71**, 683 (1987)